Supporting Information

Yeh et al. 10.1073/pnas.1010744108

SI Materials and Methods

Inhibition of Tumor Cell Growth in Vitro. Cells were grown in flasks with DMEM/F-12 medium supplemented with 10% FBS and antibiotics at 37 °C in a humidified atmosphere with 5% CO_2. Cells were kept in the log phase of proliferative activity. The sensitivity of tumor cells to iressa in the culture medium was assessed by incubating the cells in 96-well plates (Nunc) for 2 d in the presence of different concentrations of iressa and measuring the degree of tumor cell growth inhibition using the water-soluble tetrazolium (WST) colorimetric assay (Cat #TA KMK400; Fisher Scientific). Absorbance was measured at 450 nm using the Safire microplate spectrophotometer (Tecan). The data were analyzed using the software package Prizm v.4 (GraphPad Software, Inc).

ELISA for EGF Receptor. The cells were grown until 50% confluent and then harvested by scraping. Cells were pelleted, frozen on dry ice, and then thawed and lysed in a buffer (500 μL/100 mg cells) containing 20 mM Tris·HCl, pH 7.4, 150 mM NaCl, 1 mM EDTA, 1 mM EGTA, 1 mM β-glycerophosphate, 1 mM Na_3VO_4, 1 mM NaF, Triton X-100 1%, and protease inhibitor mixture 10 μL/mL (all reagents from Sigma-Aldrich) for 1 h at 4 °C. The lysate was then sonicated 3 × 10 s on ice and cleared by 14,000 × *g* centrifugation at 4 °C for 10 min. Protein concentration in the supernatant was measured by BCA Protein Assay (Thermo Scientific). Equal amounts of protein (in 100 μL volume) were added into a high binding capacity 96-well plate (Corning) and incubated for 1 h at room temperature (RT). Then, the lysate was removed, and 300 μL protein-free blocking buffer (Thermo Scientific) were added to each well for 1 h at room temperature; then, the wells were washed and incubated with antibodies against C terminus or phoshpo-tyrosine 845 of EGF receptor (EGFR; Santa Cruz Biotechnology). Incubation was terminated by washing the wells five times with PBS. HRP-conjugated secondary antibodies (Santa Cruz Biotechnology) were added for 1 h, and then, the wells were washed five times with phosphate buffer saline tween-20 (PBS-T). Colorimetric reaction was initiated by adding Ultra tetramethylbenzidine (TMB)-ELISA substrate (Thermo Scientific) and stopped by adding 2 M H_2SO_4. Absorbance was measured at 450 nm using the Safire microplate spectrophotometer (Tecan). The data were analyzed using the software package Prizm v.4 (GraphPad Software, Inc).

Irreversible Binding of 4-[(3-iodophenyl)amino]-7-{2-[2-{2-(2-[2-{2-([^{18}F]fluoroethoxy)-ethoxy}-ethoxy]-ethoxy)-ethoxy}-ethoxy]-quinazoline-6-yl-acrylamide to Active Mutant EGFR Kinase Domain. The H3255, H441, PC14, and H1975 cell lines expressing WT, L858R, and L858R/T790M mutant EGFRs were used to investigate irreversible covalent binding of 4-[(3-iodophenyl)amino]-7-{2-[2-{2-(2-[2-{2-([^{18}F]fluoroethoxy)-ethoxy}-ethoxy]-ethoxy)-ethoxy}-ethoxy]-quinazoline-6-yl-acrylamide ([^{18}F]F-PEG6-IPQA) to the EGFR kinase domain. The cells were grown in 15-cm culture dishes until 60–70% confluent and then incubated for 30 min in fresh culture medium supplemented with 20% FCS and [^{18}F]F-PEG6-IPQA at 0.37 MBq/mL. Next, the cells were washed with PBS, harvested in PBS by scraping, and pelleted by centrifugation at 400 × *g* for 5 min; the supernatant was removed, and the cell pellet was frozen on dry ice. Then, the cell pellet was thawed and lysed in the same lysis buffer as described above (200 μL/100 mg cells) for 1 h at 4 °C. The lysate was sonicated at 3 × 10 s on ice and cleared by centrifugation (14,000 rpm) at 4 °C for 10 min. The supernatant was denatured by heating at 70 °C with lithium dodecyl sulfate (LDS) sample buffer (Invitrogen) and separated by SDS/polyacrylamide gel electrophoresis using precast 4–12% Tris·HCl gel cassettes (Invitrogen). After transferring proteins onto a nitrocellulose membrane using a semidry electroblotting device (Invitrogen), the membrane was exposed to HyBlot CL autoradiography film (Denville Scientific) for 12 h to visualize the [^{18}F]-labeled protein bands. Then, the membrane was immunostained with a goat polyclonal antibody to C terminus of EGFR (Santa Cruz Biotechnology) and visualized using the ECL kit (Bio-Rad). The colocalization of [^{18}F]-labeled protein bands in the autoradiogram with protein bands stained with anti-EGFR antibody was assessed using the image analysis software MCID Analysis Rev.7.0 (InterFocus Imaging Ltd).

EGFR Kinase Assay. Biotinylated $(Gly)_4$-Tyr peptide (Upstate Biotechnologies), 0.1 mg/mL in 100 mM sodium bicarbonate buffer (pH 8.0), was incubated for 2 h in streptavidine-coated 96-well plates (Costar); nonspecific binding sites were blocked by incubation with 300 μL 3% BSA for 1 h. Tyrosine phosphorylation was initiated by adding to each well 50 ng recombinant WT EGFR, L858R EGFR, or L858R/T790M EGFR (Upstate Biotechnologies) in 100 μL assay buffer (20 mM Tris, pH 7.4, 10 mM $MgCl_2$, 1 mM $MnCl_2$, 0.2 mM ATP, 1 mM dithiothretiol, 25 mM β-glycerol phosphate, 1 mM sodium orthovanadate, 5 mM EGTA) (Sigma-Aldrich) and incubating for 30 min at 37 °C. Different concentrations of F-PEG6-IPQA were added simultaneously with the enzyme to assess dose-dependent inhibitory activity against different EGFRs. Phospho-tyrosine residues were detected by incubation with antiphosphotyrosine HRP-conjugated antibodies for 1 h at room temperature. Colorimetry was initiated by adding tetramethylbenzedine (Pierce Biotechnology), and 10 min later, the absorbance at 450 nm was measured using microplate reader Safire (Tecan). Washing with PBS (5 × 300 μL) was performed after each step.

s.c. Tumor Xenografts. s.c. tumor xenografts were established in the shoulder regions of nu/nu mice (Charles River) using the four nonsmall cell lung carcinomas (NSCLC) cell lines: H441, H3255, H1975, and PC14 ($n = 6$ per pair of cell lines and per experimental condition). Two tumor xenografts were established in each mouse in opposite shoulder regions (H441 and H3255 or H1975 and PC14) to facilitate direct comparisons of [^{18}F]F-PEG6-IPQA accumulation in tumors expressing WT EGFR and different EGFR mutants. When tumors grew to about 5–8 mm in diameter, the animals were used for in vivo imaging studies.

PET Image Acquisition and Data Analysis. The mice were gas-anesthetized (2% isoflurane per 98% oxygen mixture) and injected with [^{18}F]F-PEG6-IPQA (7.4 MBq/150 μL) through the tail vein. Whole-body dynamic PET images were acquired in a 2D mode for 2 h on a small-animal PET/CT scanner INVEON (Siemens) followed by a static scan at 3 h postradiotracer administration. Images were reconstructed using the ordered subset expectation maximization (OSEM) algorithm. The PET images were corrected for attenuation using CT imaging data using the manufacturer's software. Regional radioactivity concentration (KBq per milliliter) of [^{18}F]F-PEG6-IPQA was estimated from the maximum pixel values within regions of interest (ROI) drawn around the tumors or individual organs and tissues on transaxial slices of the reconstructed image sets. The radioactivity concentration (KBq per milliliter and μCi per milliliter) was converted to percent injected dose (ID) per gram, and the mean and SD values of radiotracer accumulation in tumors and various tissues were calculated.

Quantification of Dynamic PET Imaging Using Patlack and Logan Graphical Analyses. Because of the irreversible and covalent nature of binding of [^{18}F]F-PEG6-IPQA to the active kinase domain of EGFR, we used Patlak graphical analysis (1, 2) to calculate the rate of [^{18}F]F-PEG6-IPQA accumulation in different tumors. We used the heart-derived blood time-activity curve (TAC) as an input function between 0 and 30 min, because a previous study showed that blood radioactivity during the first 30 min post-i.v. injection of [^{18}F]F-PEG6-IPQA is predominantly caused by the parent unmetabolized compound. The Patlak plot is described by the equation (Eq. **S1**)

$$\frac{C_{Tissue}(t)}{C_p(t)} = K\frac{\int_0^t C_p(\tau)d\tau}{C_p(t)} + V, \qquad \textbf{[S1]}$$

where C_{Tissue} is the radioactivity concentration in the tissue of interest (i.e., tumor) and C_p is the radioactivity concentration in plasma. The slope of the Patlak plot represents the unidirectional influx rate constant K_i, whereas the intercept V equals $V0 + vB$ with the distribution volume $V0$ of the reversible compartment and the fractional blood volume vB.

Also, the dynamic PET imaging data were analyzed using Logan's model-independent graphical analysis (3) to assess whether [^{18}F]F-PEG6-IPQA PET/CT could be used to detect differences in expression of active mutant EGFR in tumors. The ratio of integrated radioactivity concentration in tumors over time normalized by the radioactivity concentration at a given time point in tumor radioactivity concentration was set as the y axis. The ratio of integrated reference tissue radioactivity concentration over time normalized by tumor radioactivity concentration was set as the x axis of a Logan plot. The muscle was used as reference tissue, because it has low EGFR expression. The slope of the linear portion of the Logan plot is the distribution volume ratio (DVR). If metabolite-corrected plasma TACs are not available, the plasma TAC can be replaced with reference region TAC, $C_r(t)$. Then, the slope of the linear portion of the lot is calculated as (Eq. **S2**)

$$\frac{\int_0^t C_{muscle}(t)dt}{C_{muscle}(T)} = DVR\,\frac{\int_0^t C_{tumor}(t)dt}{C_{muscle}(T)} + C. \qquad \textbf{[S2]}$$

The binding potential (BP) can be calculated as (Eq. **S3**)

$$BP = DVR - 1. \qquad \textbf{[S3]}$$

Quantitative Autoradiography. After PET imaging, the mice were killed, and the tumors were extracted rapidly, frozen, and embedded in the M1 mounting medium (Shandon-Lipshaw). Serial 20-μm-thick coronal frozen sections were cut at −13 °C using a CM3050S cryomicrotome (Leica). Tissue sections were thaw-mounted on poly-A lysine-coated glass slides and heat-fixed for 5 min at 65 °C on a slide warmer (Fischer Scientific). For quantitative autoradiography (QAR), one set of tissue sections was exposed for 6–8 h to the BAS SR-2040 phosphor imaging plate (Fujifilm) along with a set of 20-μm autoradiographic standards of known ^{18}F radioactivity concentration freshly prepared using calf liver homogenate. Images were acquired using a phosphorimager system FLA5100 (Fujifilm). Using the known radioactivity concentration in the standards and the injected dose, the autoradiographic images were converted to color-coded parametric images of percent ID per gram tissue using image analysis software MCID Elite 7.0 (InterFocus Imaging Ltd). Another set of tissue sections adjacent to those used for QAR was stained with H&E.

In Silico Modeling of [^{18}F]PEG6-IPQA Binding to EGFR. ***Methods.*** Ligand docking studies were carried out using Molecular Operating Environment (MOE) 2008.10 software (Chemical Computing Group). Structures of the cytoplasmic kinase domain of EGFR used for docking experiments with PEG6-IPQA were downloaded from the Protein Data Bank. The model for the inactive conformation of EGFR was derived from the lapatinib-bound structure 1XKK, and the gefitinib-bound L858R structure 2ITZ was used as the active conformation of the EGFR kinase domain for the docking configuration studies. The coordinates for the alternate binding mode structure were kindly provided by Michael Eck (Harvard Medical School, Boston, MA) (4). The structure of the double L858R/T790M mutant domain was constructed by replacing the side chain of T790 with that of methionine in 2ITZ. Contact constraints were removed by minimizing the structure through a steep gradient using the AMBER99 force field in the energy minimize function of MOE.

Before docking, the structures were protonated using the using the Protonate3D command of MOE. The active site was broadly defined based on residue proximity (≤4.5 Å) to the binding conformation of both ATP and gefitinib to include the probability of docking in either conformation, and it was graphically delineated with Gaussian contact surfaces. The water molecules in the vicinity of the active site were retained. The structure of PEG6-IPQA was constructed by modifying the structure of gefitinib using the builder feature of MOE, adding hydrogen atoms, and minimizing the final structure using the steepest descent algorithms. Rigid receptor-flexible ligand docking was performed using the dock simulation feature of MOE. Ligands were docked into the active and inactive EGFR kinase domain structures. The triangle matcher placement method was used to generate docking poses, and each conformation was scored based on the London ΔG scoring function that estimates the free energy of binding (kilocalories per mole).

Results. Docking results have shown that F-PEG6-IPQA can bind to both inactive and active L858R mutant forms of the EGFR kinase domain, adopting a conformation similar to gefitinib. However, the binding affinity of F-PEG6-IPQA to the active L858R mutant EGFR kinase was considerably higher, as indicated by the calculated free energy of binding of −22.8 and −16.1 kcal/mol for the active and inactive conformations, respectively (Fig. S7 *A* and *B*). This may partly be because of the more favorable van der Waals interactions with the 3-iodo aniline group in the back of the ATP binding pocket present only in the active conformation. Higher affinity of F-PEG6-IPQA to the active L858R mutant EGFR may also be attributed to an alternate binding mode similar to that reported by Yun et al. (4) for gefitinib in the L858R mutant structure. Such an alternate binding mode results in a higher gefitinib binding affinity, where the aniline ring of the inhibitor is rotated 180°, positioning the metachlorine at close proximity to the side chain of Asp855 to form a halogen bond. Such binding mode may be preferred in active mutant variants but cannot occur in the inactive WT EGFR kinase, because the required reorientation of the Asp855 is hindered by the presence of leucine at position 858. Similarly, we have found that F-PEG6-IPQA can dock in this alternate mode at a higher binding affinity (−23 kcal/mol), where the iodoaniline group is rotated 180° to interact with Asp855 (Fig. S7*C*). F-PEG6-IPQA was also able to dock into the L858R/T790M EGFR kinase in correct binding conformation. However, the calculated binding free energy of −16.9 kcal/mol was higher than that observed for the L858R mutant, indicating a lower binding affinity (Fig. S7*D*).

In silico modeling also revealed potential interactions of F-PEG6-IPQA with other EGFR active site residues. The docking conformation of F-PEG6-IPQA illustrates its covalent bonding potential with Cys797 of the active site (Fig. S7*B*). The acrylamide moiety of the F-PEG6-IPQA rests less that 1.5 Å from the ter-

minal sulfhydryl group of Cys797 to conceivably form a thiol bond. The hydrophilic PEG6 chain of the molecule is externally localized where it can interact with the outer hydrophilic surface of the binding pocket. Multiple docking iterations show that the PEG6 chain can assume many different configurations because of the rotational freedom around the single bonds in the chain. Most of those configurations, however, help to orient the rest of the molecule in the binding site, which results in a closer positioning of the acrylamide moiety in relation to the Cys797 and facilitates the alkylation reaction and covalent bond formation.

1. Patlak CS, Blasberg RG (1985) Graphical evaluation of blood-to-brain transfer constants from multiple-time uptake data. Generalizations. *J Cereb Blood Flow Metab* 5: 584–590.
2. Wu HM, et al. (2003) Measurement of the global lumped constant for 2-deoxy-2-[^{18}F] fluoro-D-glucose in normal human brain using [^{15}O]water and 2-deoxy-2-[^{18}F]fluoro-D-glucose positron emission tomography imaging. A method with validation based on multiple methodologies. *Mol Imaging Biol* 5:32–41.
3. Logan J, et al. (1996) Distribution volume ratios without blood sampling from graphical analysis of PET data. *J Cereb Blood Flow Metab* 16:834–840.
4. Yun CH, et al. (2007) Structures of lung cancer-derived EGFR mutants and inhibitor complexes: Mechanism of activation and insights into differential inhibitor sensitivity. *Cancer Cell* 11:217–227.

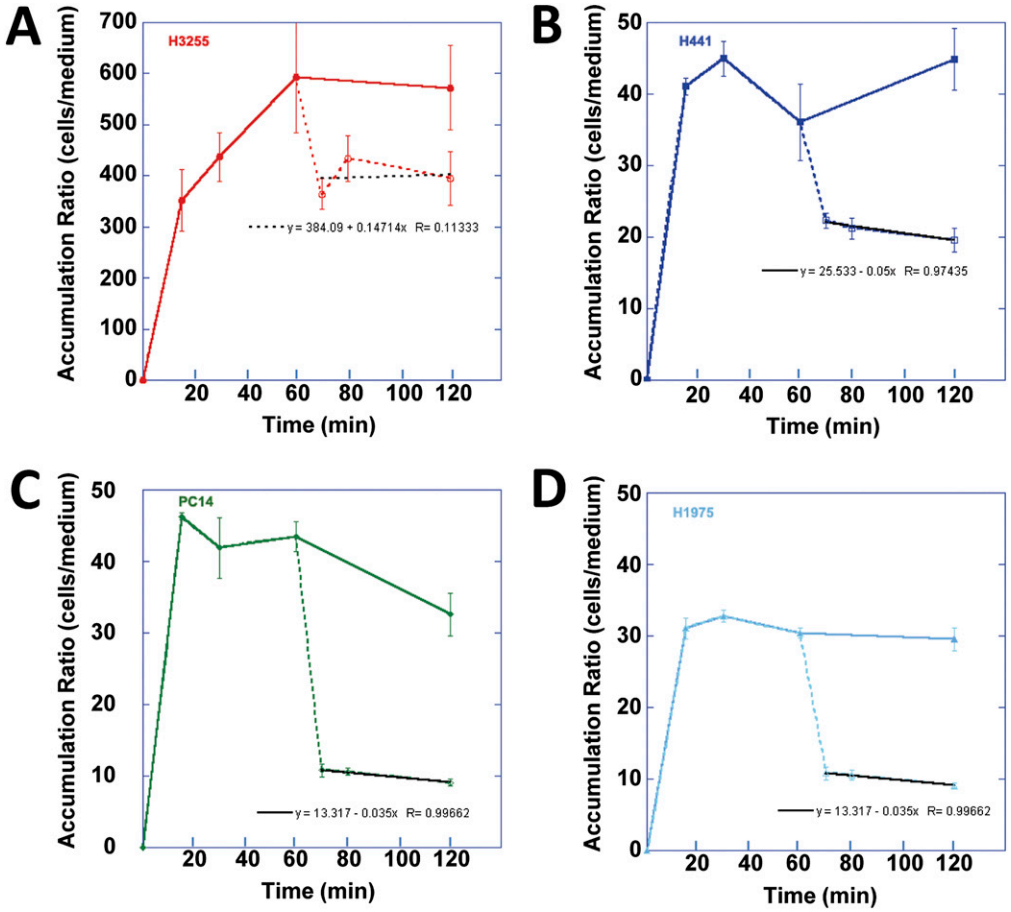

Fig. S1. Time-dependent accumulation and washout of [^{18}F]-PEG6-IPQA in vitro in different NSCLC cell lines: H3255 (*A*), H441 (*B*), PC14 (*C*), and H1975 (*D*). Linear fits of radioactivity accumulation data points between 70 and 120 min show only insignificant additional washout of [^{18}F]-PEG6-IPQA–derived radioactivity from the cells after the initial washout phase (60–70 min).

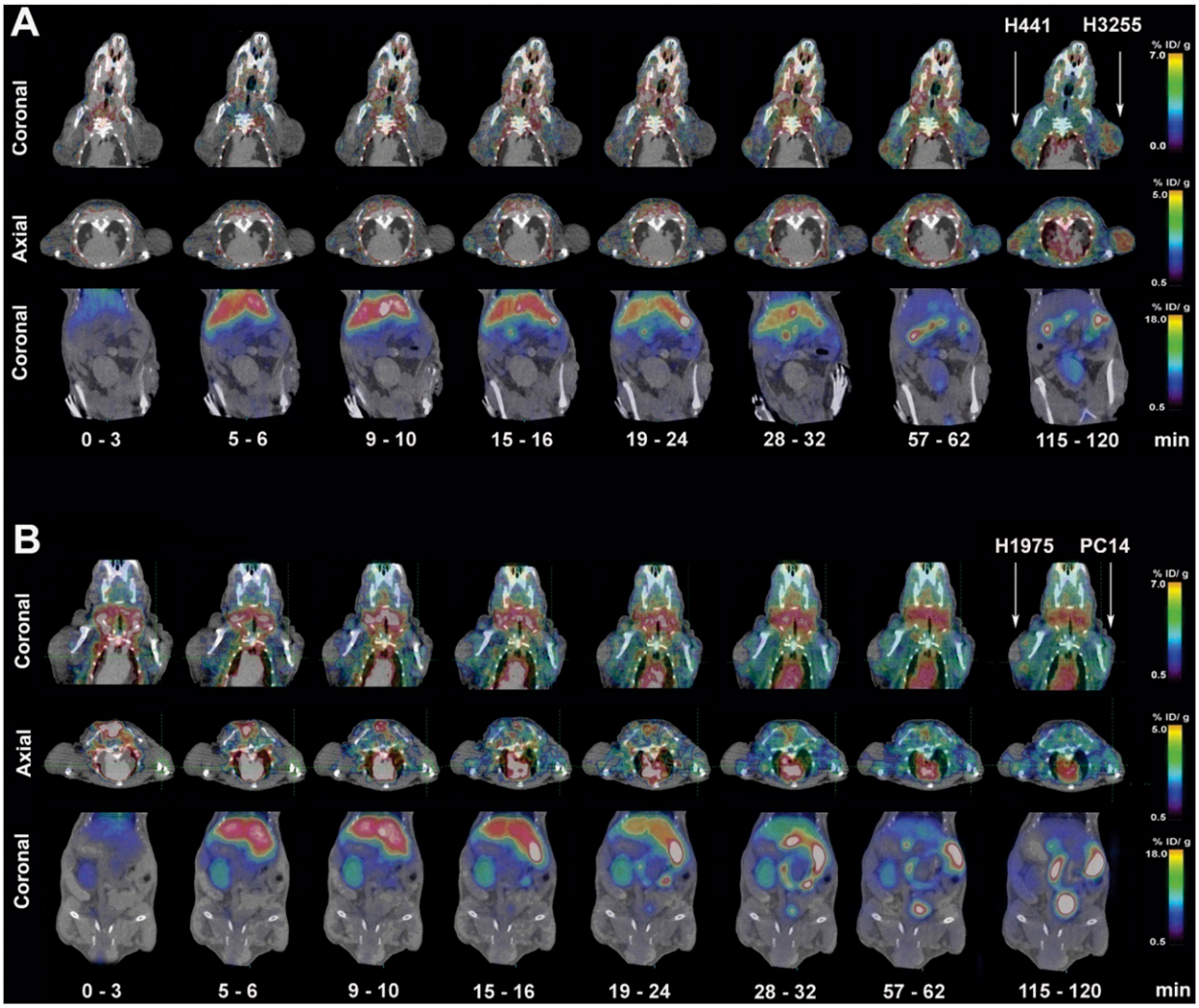

Fig. S2. Serial PET/CT images of temporal dynamics of [^{18}F]PEG6-IPQA–derived radioactivity distribution in mice bearing in the opposite shoulders: (*A*) H441 and H3255 and (*B*) PC14 and H1975 s.c. tumor xenografts (arrows). Representative PET/CT images of tumors are provided in coronal and axial planes with color coding of the range of ^{18}F]PEG6-IPQA–derived radioactivity accumulation between 0% and 7% ID/g to maximize the visualization of tumors; the corresponding coronal PET/CT images of the abdomen from the same animal are provided below and are color-coded in the range of 0.5–18% ID/g to prevent color saturation of the images.

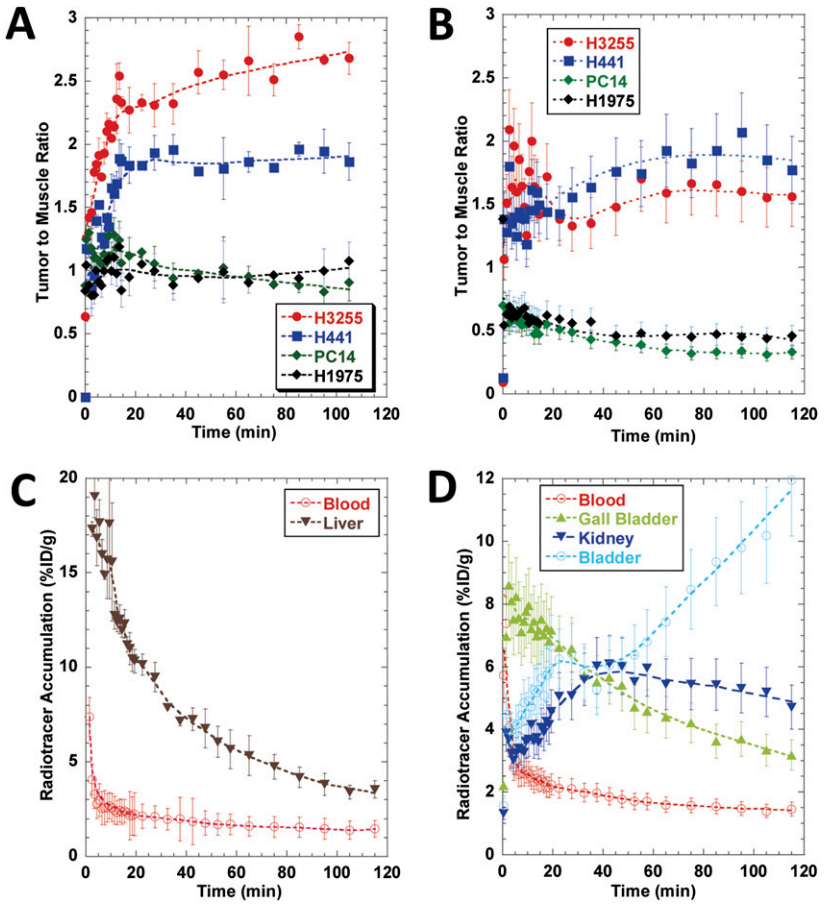

Fig. S3. Tumor to muscle ratios over time post-[^{18}F]PEG6-IPQA administration (*A*) before and (*B*) after pretreatment with iressa. Tumors: H3255 (red circles), H441 (blue circles), PC14 (green diamonds), and H1975 (light blue diamonds); muscle (brown open circles) is shown for reference. Panels *C* and *D* show time-activity curves of [^{18}F]F-PEG6-IPQA–derived radioactivity (percent ID per gram) in blood and different organs: liver (punk open squares), gall bladder (green triangles), kidney (orange circles), bladder (blue diamonds); blood (red circles) is shown for reference.

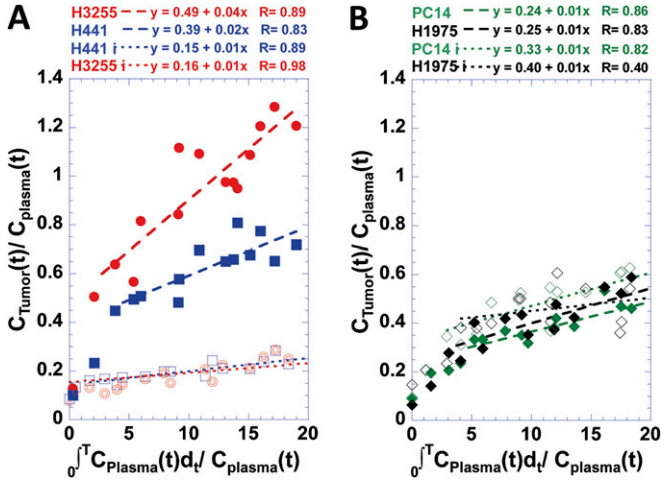

Fig. S4. The rate of unidirectional accumulation (K_i) of [^{18}F]PEG6-IPQA in different tumors was determined using Patlak graphical analysis before and after pretreatment with iressa. (*A*) Representative data from the same animals bearing H3255 (red) and H441 (blue) tumors before (filled symbols) and after pretreatment with iressa (open symbols); (*B*) representative data from the same animals bearing PC14 (green) and H1975 (blue) tumors before (filled symbols) and after pretreatment with iressa (open symbols). Linear fit equations of the data are provided above each plot.

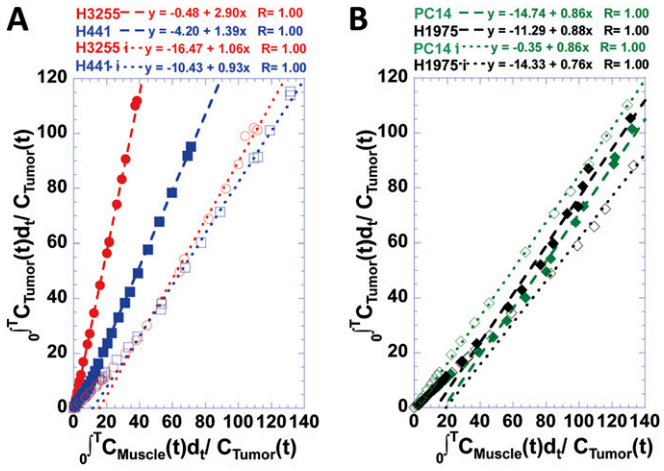

Fig. S5. The binding potential (BP) of [^{18}F]PEG6-IPQA in different tumors was determined using Logan model-independent graphical analysis before and after pretreatment with iressa. (*A*) Representative data from the same animals bearing H3255 (red) and H441 (blue) tumors before (filled symbols) and after pretreatment with iressa (open symbols); (*B*) representative data from the same animals bearing PC14 (green) and H1975 (blue) tumors before (filled symbols) and after pretreatment with iressa (open symbols). Linear fit equations of the data are provided above each plot.

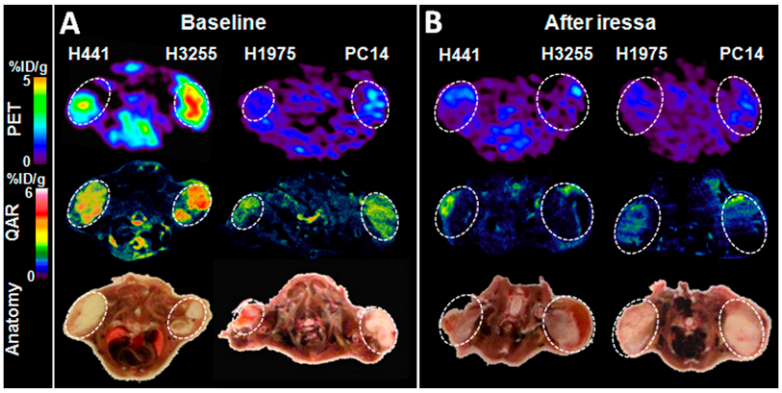

Fig. S6. Comparison of PET and quantitative autoradiographic (QAR) images of [^{18}F]F-PEG6-IPQA–derived radioactivity accumulation obtained from approximately the same area in different tumors (*A*) before and (*B*) after pretreatment with iressa. Photographs of the face of the cryosectioned block are provided for the corresponding QAR images in the bottom row; tumor areas are identified by the white dotted circles.

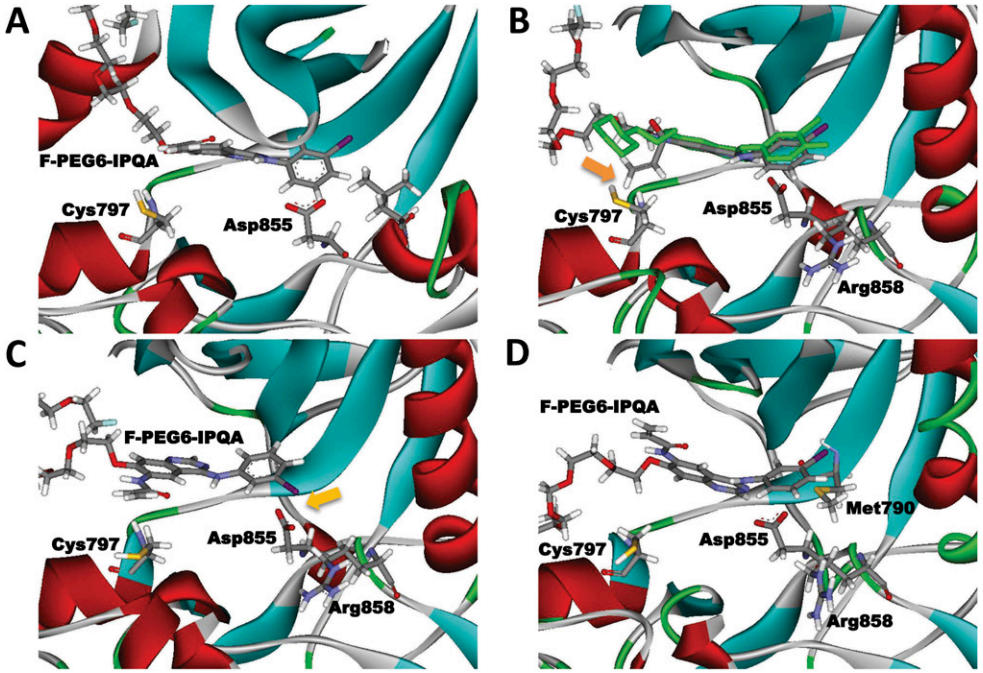

Fig. S7. In silico docking of F-PEG6-IPQA with the WT (*A*), active L858R mutant (*B* and *C*), and TKI-resistant L858R/T790M double-mutant EGFR kinase. F-PEG6-IPQA can bind to both active WT (*A*) and L858R mutant (*B*) forms of the EGFR kinase domain in a conformation similar to gefitinib (green structure). This conformation places the acrylamide moiety of F-PEG6-IPQA in close proximity to the sulfhydryl group of Cys797 (orange arrow). F-PEG6-IPQA can also bind to the L858R mutant in an alternate conformation where the aniline ring of the substrate is rotated 180°, positioning the metaiodine (yellow arrow) at close proximity to the side chain of Asp855 (*C*). F-PEG6-IPQA can also dock into the active site of the L858R/T790M double mutant in the correct conformation (*D*), albeit with a higher calculated binding energy, which indicates a weaker binding affinity.